IOSR Journal of Business and Management (IOSR-JBM)
e-ISSN:2278-487X, p-ISSN: 2319-7668. Volume 26, Issue 5. Ser. 6 (May. 2024), PP 52-61
www.iosrjournals.org

Analysis And Analytic Optimization Of A Resonance Fatigue Test Rig

Artur Cantisano[1], Luiz Guilherme Aun Fonseca[2], Ronnie Rodrigo Rego[3], Jefferson De Oliveira Gomes[4]

[1]*instituto Tecnológico De Aeronáutica, São José Dos Campos, Brasil*
[2]*instituto Tecnológico De Aeronáutica, São José Dos Campos, Brasil*
[3]*instituto Tecnológico De Aeronáutica, São José Dos Campos, Brasil*
[4]*instituto Tecnológico De Aeronáutica, São José Dos Campos, Brasil*

Abstract:
Fatigue tests is yet indispensable for components operating under intrinsic heavy cyclic loads. Many test rigs use the resonance phenomenon to raise test frequencies and reduce the time and cost required. Although resonance is a well-known phenomenon, there is still room for investigation regarding the influence of the power source to the system's overall capability. The objective of the present study is the introduction of the actuator's power limitations in the analytical formulation that describes the dynamic behavior of a shaft bending and torsion fatigue test rig. The electrodynamic shaker power restriction was introduced into the system and was modelled as an equivalent two degree of freedom to obtain the equations that describes the oscillatory movement. Two parameters were identified as primarily responsible for bending moment and the operating frequency change. A 27% increase in maximum bending moment compared to a baseline design was achieved by optimization. Inertia was identified as solely responsible for the increased operating frequency, and the boundary conditions for topological optimization of the inertia arms were presented. It was concluded that the effect of resonance can lead the actuator to accelerations beyond the nominal values of the manufacturer.

Keywords*: Crankshaft; Test rig; Fatigue; Resonance; System modeling.*

Date of Submission: 16-05-2024 Date of Acceptance: 26-05-2024

I. Introduction

Several recent developments in the automotive industry have fuel consumption and greenhouse gas (GHG) emissions as background [1-3]. Severe regulations regarding these aspects force automakers to seek improvements in key systems of the vehicle. On 14 July 2021, the European Commission adopted a series of legislative proposals to achieve climate neutrality in the EU by 2050. The Commission's proposal to cut greenhouse gas emissions by at least 55% by 2030 [4]. In December 2021, EPA finalized revised national greenhouse gas (GHG) emissions standards for passenger cars and light trucks. The updated standards will result in avoiding more than 3 billion tons of GHG emissions through 2050[5].

Aligned with the need to improve power and save fuel, new developments tend to accomplish that through the implementation of more than one technology. Aside from electrification, the combination of direct injection, variable valve timing, engine downsizing and turbocharging became trends, as stated by Stephenson [1]. The consequence are extra loads over the engine main components, such as the crankshaft. Furthermore, optimizing it for mass and rotational inertia represent direct gains in terms of GHG emissions. However, it also tends to reduce safety factors, possibly compromising its durability performance. For those conflicting aspects to be balanced, representative fatigue tests must be performed to verify the reliability of the engine's main components.

On the one hand, material fatigue strength can be experimentally determined through standardized rotating bending or tensile-compressive tests [6, 7]. The limitation of these procedures lies on the difficulty to reproduce the operational efforts and exact manufacturing conditions to the standard specimens. Engine dynamometer tests, on the other hand, provide real operational loading to the components. The restrictions lie in the equipment's capacity to lead a specific component to fatigue failure without the influence of other engine components. Therefore, to aggregate enough mechanical effort to reach the material's endurance limit and simulate real operational conditions, the solution resides in dedicated machines for each single component.

Crankshaft design is challenging not only because of its complex geometry, but also because of the extreme loads that it is subjected to. From a mechanical effort point of view, during a combustion cycle, the crank journals experience mainly bending, while the main journals are subjected almost only to torsion, as explained by Fonte et al. [8].

According to Huertas et al. (2017) the most appropriate equipment for fatigue testing is the resonant plate test bench system, because it can induce high moments with high frequencies [9]. With this configuration, as stated by Feng and Li (2003) [10], experimental time can be drastically reduced in comparison to other alternatives, due to testing frequencies up to 100 Hz. A similar configuration was also used by Yu et al. (2004) [11], who studied the resonance frequency shift due to notches induced at the crankshaft bearing. Results related to frequency drop during tests were used in a correlation with crack appearance in crankshafts. With the same machine, Chien et al. [12] and Spiteri et al. [13] also developed studies on aspects related to deep rolling, a crankshaft manufacturing process. Similarly, Ko et al. [14] investigated alterations of surface hardening treatments in the fatigue life of crankshafts using a resonance test rig. Followed by that, Ho et al. [15] created a correlation between stress distribution and bending moment on specimens tested.

The study performed by Williams and Fatemi [16] developed a test rig with a different concept, utilizing a servo-hydraulic actuator instead of a motor or an electrodynamic shaker. The drawback related to this configuration is the long period taken by fatigue experiments to be made. Bending and torsion moments were applied to a V8 diesel crankshaft throw in the research done by Villalva and Ferracini [17]. A correlation between data acquired from extensometers positioned in the test rig and finite element bending simulations could be reached. Similar procedure was done by Baragetti et al. [18] to investigate nitriding improvement to crankshaft fatigue. The staircase test methodology was utilized by Çevik and Gürbüz [19] to conduct resonant bending fatigue tests with cast iron diesel crankshafts. Stress versus number of cycles and endurance limit could be determined for rolled and unrolled conditions.

The research conducted by Huertas et al. [9] brings a summary on the state of the art of the technologies employed in test rig systems used to evaluate shaft fatigue resistance. The authors developed an optimization model to select the inertia block configuration that maximizes the test frequency at the same time as respects design constraints. However, this study does not take into consideration the dynamic response of the test rig, as the authors proceeded with their design at static condition.

Despite being widely used by the industry, there is still lack of public knowledge related to crankshaft test rig development and capacity. This survey on the state-of-the-art reveals that, although test rigs are extensively used to investigate component fatigue, they do not explore all aspects related to the dynamic behavior of such rigs. Existing articles do not cover all equipment parameters and system performance details. A gap is still existent on the understanding of which variables influence the test rig capability and how they affect the test rig operational behavior under a dynamic perspective. This study proposes to contribute with on-going fatigue related experiments optimization and in the development of new resonant test rigs.

II. Objective And Approach

The objective of this study is an analytical model proposal to optimize the dynamic behavior of a resonance fatigue test rig considering the power limitations of the actuator. The fundamental contribution is to input into the model's analytical formulation the influences of the electrodynamic shaker and thereby to propose an optimization of the parameters to reach the equipment maximum capability. The approach taken to achieve the objective starts with a brief description of the resonance fatigue test rig functional development and features. The electrodynamic shaker model used in the study is presented, along with the explanation of the parameters of interest taken from the manufacturer's experimental datasheet. A two degree of freedom system was modeled to obtain the equations that describes the forced damped oscillatory movement. The test rig operational map arises from the analysis of the maximum force and stroke length provided by the actuator. A quantitative example is given, along with a qualitative visualization of the system's operation range.

III. Test Rig And Model Development

Test rig design overview

The test rig was designed following the principles of integrated product development. The establishment of design requirements defined the functions that meet the technical specifications to reach a conceptual design for the test rig [20]. Figure 1(a) illustrates the bending configuration with all its features. Figures 1(b) and 1(c) show the bending and torsion cores assembled, respectively.

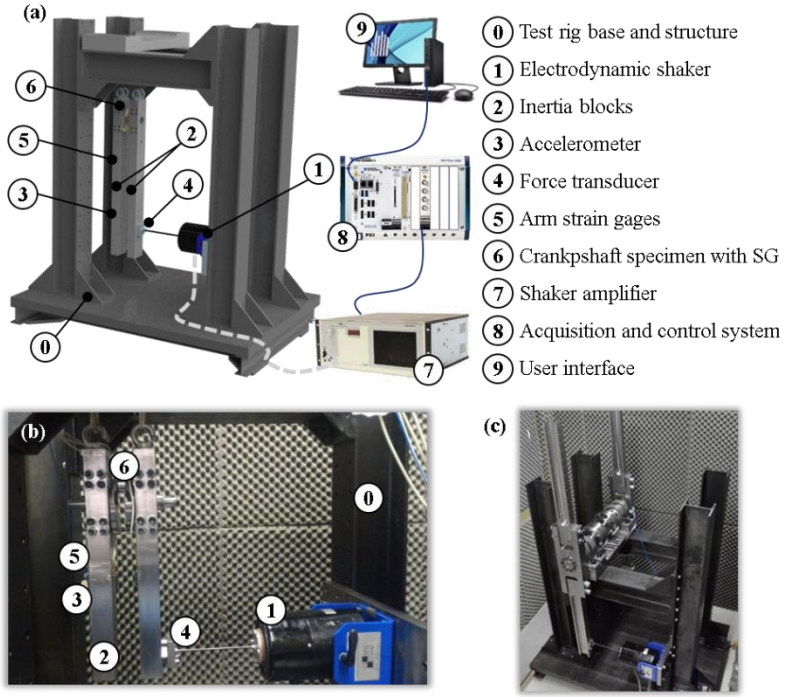

Fig. 1 (a) Test rig bending configuration core sensors, actuator, and control system; (b) bending assembly; (c) torsion assembly.

The equipment was developed to test both bending and torsional configurations using the resonance phenomenon to amplify the input loads. The crankshaft specimen is fixed to suspended inertia blocks to reduce the natural frequency and favor the desired vibration mode for testing. The bending core inertia blocks are instrumented with strain gages to transform deformation data into acting moment. The torsion core is equipped with an in-line torque transducer, giving a direct load reading. Since the shaker responds to the controlled input signal without embedded feedback, an accelerometer was positioned at the driven inertia block to provide information of the actual system acceleration. The power source is an electrodynamic shaker that excites the system with an input sinusoidal force, which is measured by a load cell. The model used along this development was the K2110E, up to 489 N of maximum sine force and 25.4 mm of stroke, manufactured by *The Modal Shop,* Inc.

Analytical modelling for the vibrating system

By determining the crankshaft's stiffness and damping coefficients, the blocks' inertia and the shaker's sinusoidal force input transformed into moment, a simplified two degrees of freedom system can be defined as follows. Specifically for the bending core, Fig. 2 shows the system's modeling with an equivalent block diagram.

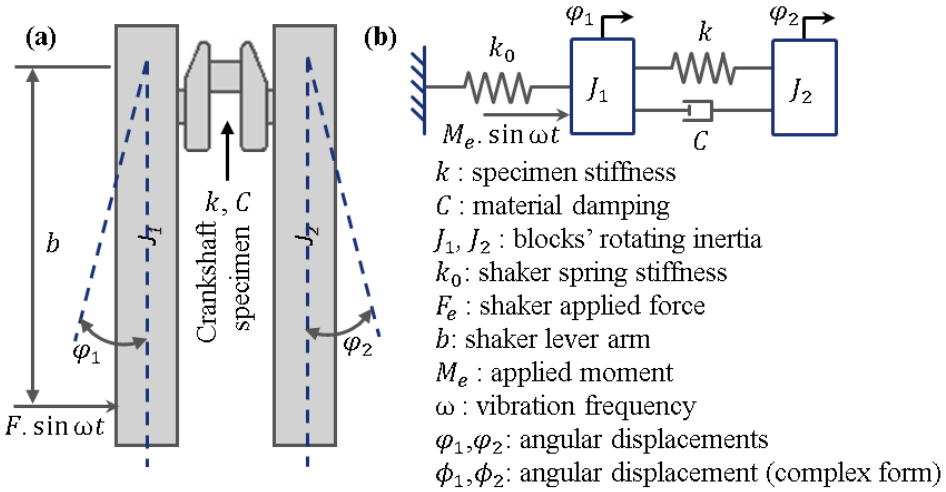

Fig. 2 (a) Sketch of the rig; (b) The equivalent diagram of vibration of the test rig [21].

The first vibrational mode is related to the joined movement between the two inertia blocks. The second mode is of interest, as it corresponds to opposite relative movement between J_1 and J_2, which leads to the application of moment to the crank specimen. Values of K and C refer to the system's stiffness and damping coefficients respectively. The external moment applied by the shaker can be translated as an amplitude of M_e with a sinusoidal function oscillating at frequency ω. The study performed by Feng and Li [10] brings the deduction of the equations, summarized as follows.

Assuming that φ_1 and φ_2 represent angular displacements of block 1 and 2 respectively, the exciting moment that the shaker applied to block 1 is $M_e \, sin \, sin \, \omega t$ and $J_1 = J_2 = J$, the differential dynamic equations can be expressed as the Eq. (1) and (2):

$$J \times \ddot{\varphi_1} + C \times (\dot{\varphi_1} - \dot{\varphi_2}) + (K_0 + K) \times \varphi_1 - K \times \varphi_2 = M_e \, sin \, sin \, \omega t \quad \text{Eq. (1)}$$

$$J \times \ddot{\varphi_2} + C \times (\dot{\varphi_2} - \dot{\varphi_1}) + K \times (\varphi_2 - \varphi_1) = 0 \quad \text{Eq. (2)}$$

Turning the Eq. (1) and (2) in the complex form, solving the system and considering the stiffness of the shaker core small compared to system stiffness ($K_0 \sim 0$), equations of amplitudes $\underline{\phi_1}$ and $\underline{\phi_2}$ are determined. Subtracting one from the other derives the movement amplitude in Eq. (4).

$$\phi = \underline{\phi_1} - \underline{\phi_2} \quad \text{Eq. (3)}$$

$$\phi = \frac{F \times b}{2 \times K \times \sqrt{(1 - r^2)^2 + 4 \times r^2 \times \xi^2}} [rad] \quad \text{Eq. (4)}$$

Where F is the shaker input force, b is the lever arm between center of rotation and shaker force application point. Multiplying Eq. (4) by the specimen according stiffness K leads to the determination of the applied bending moment (5), as demonstrated in Eq. (6).

$$M = \phi \times K \quad \text{Eq. (5)}$$

$$M = \frac{F \times b}{2 \times \sqrt{(1 - r^2)^2 + 4 \times r^2 \times \xi^2}} \; [N.m] \quad \text{Eq. (6)}$$

Replacing F by the maximum force value of the shaker, the maximum moment of the system considering the force limitation is obtained.

$$M_{force}^{max} = \frac{F_{max} \times b}{2 \times \sqrt{(1 - r^2)^2 + 4 \times r^2 \times \xi^2}} \; [N.m] \quad \text{Eq. (7)}$$

In addition to the limitation of maximum force, the shaker has the limitation of maximum operating stroke S_{max}. Considering small-angle approximations, converting S_{max} to the angle ϕ_{max}, and replacing ϕ for ϕ_{max} in Eq. (5), the maximum moment considering the stroke limitation is found in Eq. (8). Thus, it is possible to theoretically calculate the maximum bending moment generated by the system, considering the physical limitations of maximum stroke and maximum force of the electrodynamic exciter.

$$M_{stroke}^{max} = \frac{S_{max}}{b} \times K \; [N.m] \quad \text{Eq. (8)}$$

IV. Results And Discussion

The first results come from the application of the vibrational model to the existent equipment, in order to identify the parameters magnitude's influence. The system damping was estimated at 0.5%, a usual damping value for elastic deformation in materials [25]. The distance b of 0.75 m, the stiffness K of 112.226 N.m/rad and the inertia J of 0.777 kg.m³ are specific parameters for this equipment. An operational map could be created from Eq. (7) and (8) to illustrate the maximum bending moment limited, respectively, by shaker force and shaker amplitude, as shown in Fig. 3.

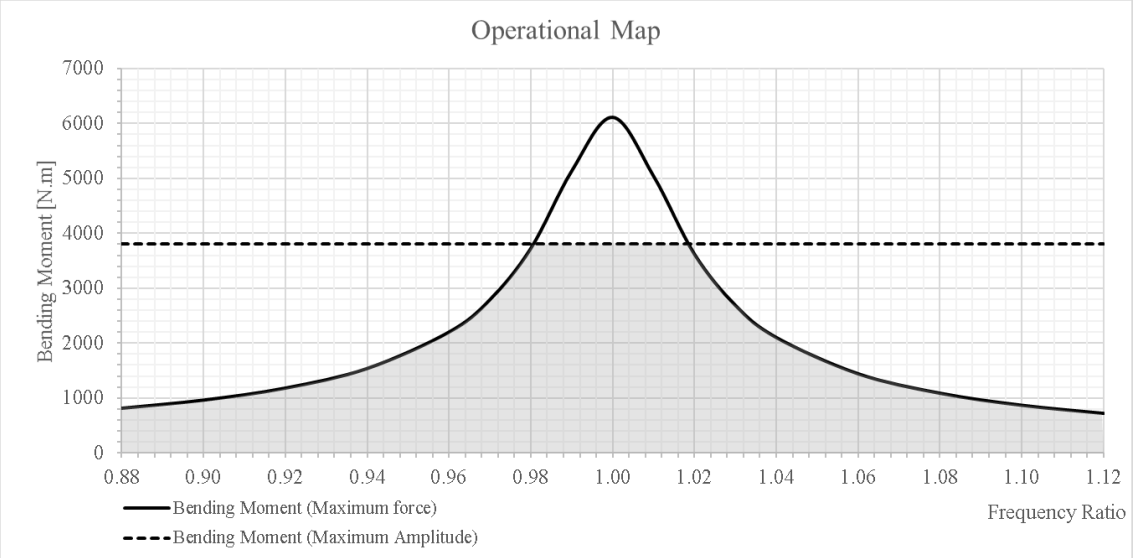

Fig. 3 Theoretical operational map of the bending configuration test rig.

As can be visualized in Fig. 3, at the same time as M_{force}^{max} reaches a peak at resonance, M_{stroke}^{max} is not influenced by the frequency ratio. Therefore, with the parameters of the actual rig, the maximum moment is limited by the maximum stroke of the shaker rather than its maximum force. In other words, the equipment can be underutilized, allowing room for optimization of its parameters to further explore its potential.

The initial optimization analysis considered the evaluation of the operating parameters, their dependency status with other components and systems and the consequence of their change in the equipment behavior. For example, when increasing the inertia reduces the operating frequency. Figure 4 summarizes the operating parameters influence over the equipment's load capacity.

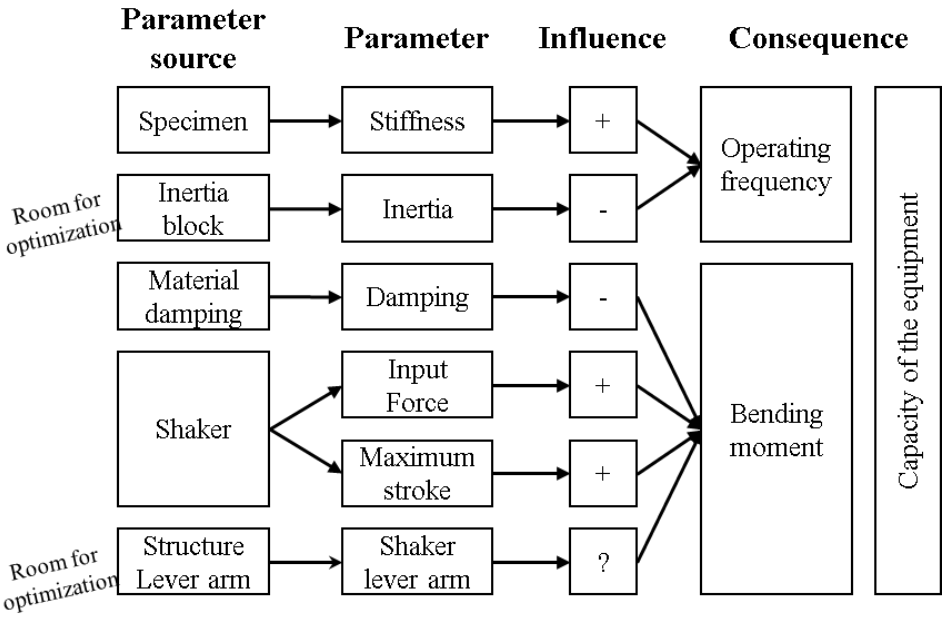

Fig. 4 Operation parameters and their analysis of dependence.

The modification of the parameters results in changes of the operating frequency and the bending moment, consequently, correspond to the equipment's capability to induce high loads at high frequencies. As a result, larger specimens can be tested in increasingly shorter periods of time.

The operating frequency is dependent on the rigidity and inertia of the system. Stiffness is primarily dependent on the specimen and its increase raises the operating frequency. In turn, the inertia is primarily dependent on the inertia block and its increase reduces the operating frequency. Considering that the specimen is not altered, the optimization of the inertia arms can increase the natural frequency and consequently the test

frequency. This allows room for optimization and improvement of the capacity of the equipment, by increasing the Operating Frequency.

The bending moment of the equipment is a consequence of damping, maximum shaker input force, maximum stroke, and the lever arm length. The damping corresponds to the intrinsic properties of materials on deformation, primarily of the specimen. Thus, the influence of damping is not the subject of the present investigation. The maximum force and stroke are consequence of the model of the selected electrodynamic shaker. Since the optimization of these parameters is limited by the individual design of each manufacturer, these parameters remain unchanged in this study. The lever arm is dependent of the designed geometry of the inertia block. The lever arm positively influences the bending moment generated by the maximum force, and negatively influences the bending moment generated by the maximum stroke. This allows room for optimization and improvement of the capacity of the equipment, by increasing the bending moment.

Inertia block force analysis

The inertia block has its main functions to transfer the excitation of the shaker through the lever arm and support the test bending moment. Figures 5(a) and 5(b) show the individualized efforts.

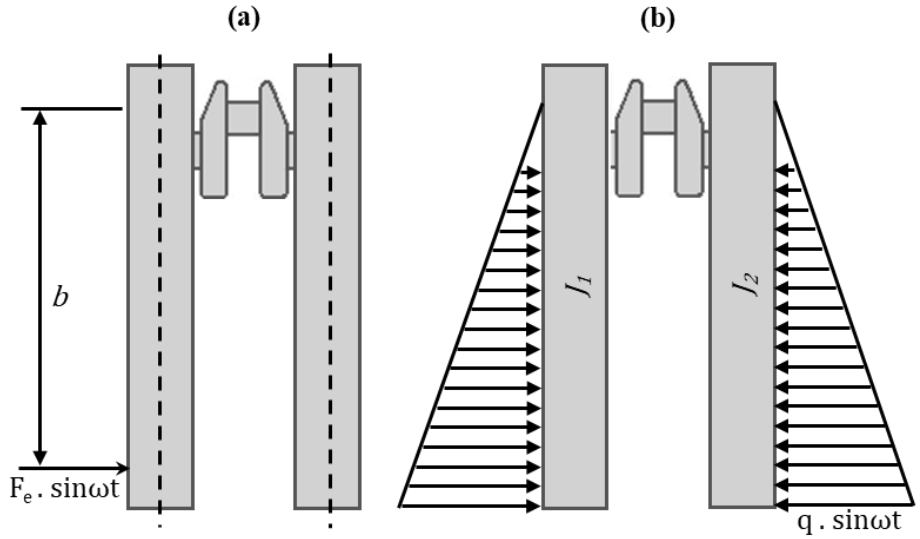

Fig. 5 (a) Excitation generated by the shaker in the spring mass system; (b) Resulting moment in the vibration system.

The moment generated during testing (Fig. 5b) is from the potential energy stored in the spring mass system. The elastic potential energy is stored in the system in the form of stress and becomes kinetic energy. The acceleration along the inertia block increases as the observation point moves away from the center of rotation. Considering a constant section along the block, one can transcribe in force the acceleration at each point as a triangular distribution (Fig. 5b). The resulting load in the inertia block is the sum of the force generated by the shaker (Fig. 5a) with the force distribution generated by the inertia of the inertia block (Fig. 5b). Thus, by changing the geometry of the inertia block, the resulting force distribution also changes. The relationship between the geometry of the inertia arm and the resulting force distribution means that there is no simple solution through an analytical analysis. Thus, by changing the geometry of the block, the resulting force distribution also changes. Therefore, a topological optimization is necessary.

Huertas et al. (2017), developed a resonance test bench and performed a topological optimization on the inertia arms. Frequencies of up to 100 Hz were achieved, with a deflection of 2 mm. Figure 6 presents the boundary conditions and the result obtained in the optimization performed [9].

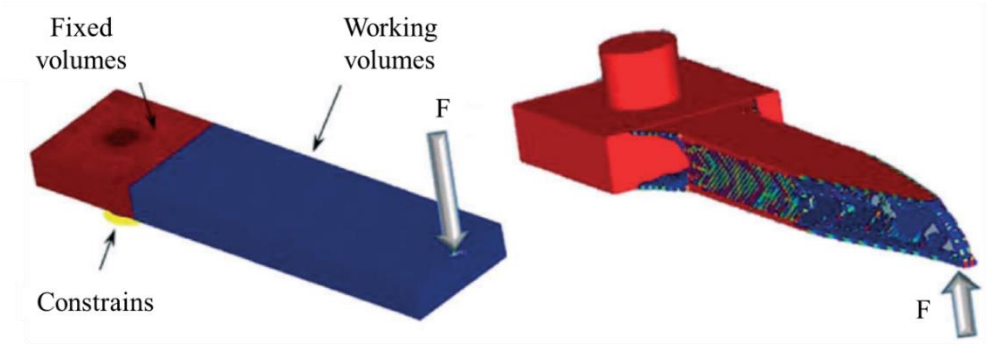

Fig. 6 Topological optimization of resonant plates: Input geometry and constraints for the topological optimization (left); Optimized topology for resonant plates (right) [9].

Despite having reached a high natural frequency of the system, the use of a force concentrated at the end of the inertia arm means that the full potential of the optimization was not reached. As previously described, the resulting efforts consist of a load distribution, and the profile of this distribution changes with mass reduction. Thus, frequencies higher than 100 Hz are estimated in a future topological optimization in which optimization cycles and force distribution recalculation are considered.

Structure lever arm optimization

An analytical optimization was performed in search of an optimum value for the lever arm. By evaluating the moments' Eq. (7) and (8) in relation to the lever arm, it can be concluded that the resulting moment will be maximum when M_{force}^{max} equals M_{stroke}^{max}, which derives Eq. (9).

$$M_{force}^{max} = M_{stroke}^{max}$$

$$\frac{F_{max} \times b}{2 \times \sqrt{(1-r^2)^2 + 4 \times r^2 \times \xi^2}} = \frac{S_{max}}{b} \times K$$

$$b = \sqrt[2]{\frac{2 \times K \times S_{max} \times \sqrt{(1-r^2)^2 + 4 \times r^2 \times \xi^2}}{F_{max}}} \quad [m] \qquad \text{Eq. (9)}$$

An optimal *lever arm* value was found according to the operating parameters. From Eq. (9), *b* becomes dependent on the stiffness, frequency ratio, damping and the values of maximum force and maximum stroke of the shaker. Using the optimal value *b* in the existing equipment, Fig. 7 shows the capacity gain achieved.

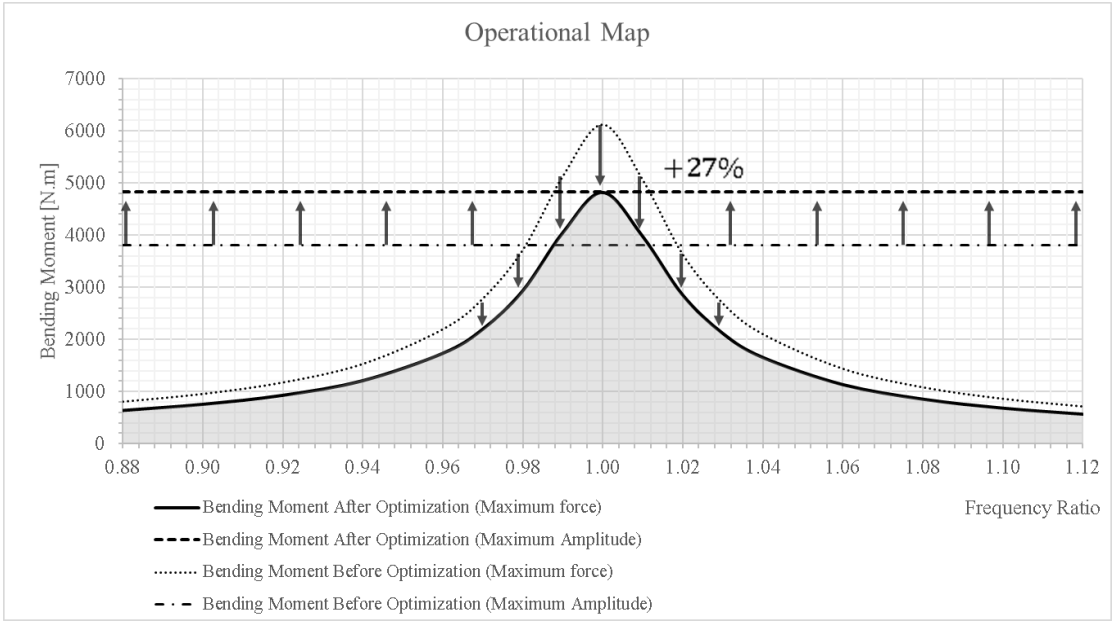

Fig. 7 Operational map with optimized lever arm.

The optimal lever arm was determined to be 0.591 m for this particular case, with which a reduction of M_{force}^{max} and an increase of M_{stroke}^{max} are obtained, consequently raising the maximum moment from 3801 N.m to 4826 N.m.

Equivalent mass model

Although the analytical model concludes that the mass inertia has no influence on the moment capacity of the equipment, this is not an intuitive conclusion. To enlighten the matter, an equivalent mass concept for the system was idealized.

The equipment's inertia blocks weight approximately 25 kg, but the equivalent mass consists only by the mass perceived by the actuator during operation. Figure 8 illustrates this approach, as the vibrational system composed by the two inertia blocks and crankshaft specimen are simplified to one equivalent mass attached to the exciter.

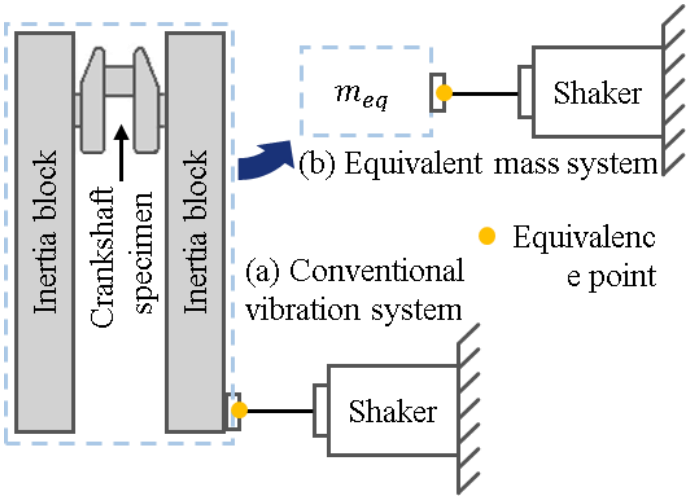

Fig. 8 Squematics for the (a) conventional vibration system and (b) equivalent mass system.

To find the equivalent mass, it was admitted an equal acceleration and force in both systems at the equivalence point. First, the maximum acceleration formula is obtained Eq. 10.

$$\left|\underline{\ddot{\varphi}_1}\right| = \left|-\omega^2 \times \underline{\phi_1}\right| \qquad \text{Eq. (10)}$$

Since it has been assumed that the inertia J_1 is equal to J_2, the displacement ϕ_1 and ϕ_2 are equal, and consequently ϕ_1 is half of the total ϕ. Eq. (11) shows the linear acceleration at the symmetry point.

$$\left|\underline{\ddot{\varphi}_1}\right| = \omega^2 \times \frac{\phi}{2}$$

$$\left|\underline{\ddot{\varphi}_1}\right| = \frac{2 \times K}{J} \times r^2 \times \frac{\frac{F \times b}{2 \times K \times \sqrt{(1-r^2)^2 + 4 \times r^2 \times \xi^2}}}{2} \left[\frac{rad}{s^2}\right]$$

$$a_{max} = \left|\underline{\ddot{\varphi}_1}\right| \times b \left[\frac{m}{s^2}\right]$$

$$a_{max} = \frac{r^2 \times F \times b^2}{2 \times J \times \sqrt{(1-r^2)^2 + 4 \times r^2 \times \xi^2}} \left[\frac{m}{s^2}\right] \qquad \text{Eq. (11)}$$

Isolating F from Eq. (11), it is possible to recognize the 2nd Newton law in Eq. (12).

$$F = a_{res} \times \frac{2 \times J \times \sqrt{(1-r^2)^2 + 4 \times r^2 \times \xi^2}}{r^2 \times b^2} [N] \qquad \text{Eq. (12)}$$

$$m_{eq} = \frac{2 \times J \times \sqrt{(1-r^2)^2 + 4 \times r^2 \times \xi^2}}{r^2 \times b^2}[kg] \quad \text{Eq. (13)}$$

Analyzing Eq. (13) it can be concluded that force, stiffness, and acceleration has no influence in the result. The equivalent mass is an index of the equipment configuration, been a percentage of the total inertia of the system. For the parameters after optimization, where $J = 0.777\ [kg.m^2]$, $\xi = 0.015$, $b = 0.591\ [m]$ and $r = 1$, the equivalent mass of the system was calculated to be 0.094 kg. This result concludes that the selected shaker is in fact overestimated.

When connecting the shaker, its mobile mass (rod) becomes part of the vibratory system, constituting part of the equivalent mass. The result is an equivalent mass less than the mass of the shaker rod itself, theoretically reaching accelerations of 545 [g], almost 5.5 times the maximum acceleration described by the manufacturer. This shows that an actuator operating in resonance can exceed its dynamic limits. It is concluded that the experimental results obtained by the shaker manufacturer are not sufficient to delimit the acceleration limit of the equipment when applied to a resonant bench. Nonetheless, by exceeding such limits set by the manufacturer, the equipment can reach the mechanical resistance of its internal components, which may not be advised.

V. Conclusion And Next Steps

An investigation was performed on a resonance fatigue test rig to identify the influence of each parameter in the equipment's capability. Two parameters were identified as primarily responsible for increasing the bending moment and the operating frequency: inertia and lever arm.

First, the reduction of the inertia of the inertia blocks increased the operating frequency without reducing the maximum bending moment reached by the equipment. The blocks are primarily responsible for the inertia of the system, and a force analysis has shown that its force distribution is dependent on its inertia. The search for a geometric optimization to reduce inertia analytically, however, was deemed unfeasible. The performance of a topological optimization is suggested at this point.

The second possible optimization parameter identified was the lever arm. The analysis performed showed that it has an influence proportional to the maximum bending moment reached by the maximum force of the shaker, and inversely proportional to the maximum bending moment reached by the maximum stroke., The ideal value of the lever arm was obtained, increasing the maximum bending moment in 27% from an initial baseline.

It could be concluded that due to the resonance and energy conservation of the system, the compensation of system losses is performed by the actuator. Thus, the inertia of the system does not influence the maximum bending moment, and the mass perceived by the actuator (0.094 kg) is significantly less than the total vibrating mass (25 kg). This conclusion may not be intuitive, as the perceived mass is even smaller than the mass of the shaker rod itself. It can be understood that the effect of resonance can lead the equipment to accelerations and frequencies beyond the nominal values of the manufacturer.

The next steps of this research are the experimental acquisition of the damping factor, the topological optimization of the inertia arm, fabrication, and testing of the optimized inertia arm. Obtaining damping will allow accurate results for the analytical model and tests for statistical validation. Topological optimization will allow to reach operating frequencies unimaginable until now.

Acknowledgements

The authors would like to thank MSc. Paulo Vieira Netto (FCA Group) for the enlightening discussions and contributions.

Funding

This study was partially funded by the Brazilian agency CNPq under grants 159026/2013-0 and 147267/2015-3 and also Coordenação de Aperfeiçoamento de Pessoal de Nível Superior (CAPES) under Grant 88881.187305/2018-01 for the Programa Institucional de Bolsas de Doutorado Sanduíche no Exterior - PDSE.

References

[1]. Stephenson, M. (2009). Engine Downsizing–An Analysis Perspective. In Simulia Customer Conference.
[2]. Bandel, W., Fraidl, G. K., Kapus, P. E., Sikinger, H., & Cowland, C. N. (2006). The Turbocharged Gdi Engine: Boosted Synergies For High Fuel Economy Plus Ultra-Low Emission (No. 2006-01-1266). Sae Technical Paper. Https://Doi.Org/10.4271/2006-01-1266
[3]. Nishida, K., Sakuyama, H., & Kimijima, T. (2009). Improvement Of Fuel Economy Using A New Concept Of Two-Stroke Gasoline Engine Applying Stratified-Charge Auto-Ignition (No. 2009-28-0009). Sae Technical Paper. Https://Doi.Org/10.4271/2009-28-0009
[4]. European Commission. 2030 Climate Target Plan. Available At: Https://Ec.Europa.Eu/Clima/Eu-Action/European-Green-Deal/2030-Climate-Target-Plan_En. Accessed 22 April 2023
[5]. United States Environmental Protection Agency (2022). Final Rule To Revise Existing National Ghg Emissions Standards For Passenger Cars And Light Trucks Through Model Year 2026. Available At: Https://Www.Epa.Gov/Regulations-Emissions-Vehicles-And-Engines/Final-Rule-Revise-Existing-National-Ghg-Emissions. Accessed 2 April 2022

[6]. Iso 1143:2010 Metallic Materials - Rotating Bar Bending Fatigue Testing
[7]. Iso 12106:2017 Metallic Materials - Fatigue Testing - Axial-Strain-Controlled Method
[8]. Fonte, M., Li, B., Reis, L., & Freitas, M. (2013). Crankshaft Failure Analysis Of A Motor Vehicle. Engineering Failure Analysis, 35, 147-152. Https://Doi.Org/10.1016/J.Engfailanal.2013.01.016
[9]. Huertas, J. I., Navarrete, N., Giraldo, M., Uribe, J. D., & Gasca, J. J. (2017). Resonant Fatigue Test Bench For Shaft Testing. Fatigue & Fracture Of Engineering Materials & Structures, 40(3), 364-374. Https://Doi.Org/10.1111/Ffe.12500
[10]. Feng, M., & Li, M. (2003). Development Of A Computerized Electrodynamic Resonant Fatigue Test Machine And Its Applications To Automotive Components (No. 2003-01-0951). Sae Technical Paper. Https://Doi.Org/10.4271/2003-01-0951
[11]. Yu, V., Chien, W. Y., Choi, K. S., Pan, J., & Close, D. (2004). Testing And Modeling Of Frequency Drops In Resonant Bending Fatigue Tests Of Notched Crankshaft Sections. Sae Transactions, 619-627.
[12]. Chien, W. Y., Pan, J., Close, D., & Ho, S. (2005). Fatigue Analysis Of Crankshaft Sections Under Bending With Consideration Of Residual Stresses. International Journal Of Fatigue, 27(1), 1-19. Https://Doi.Org/10.1016/J.Ijfatigue.2004.06.009
[13]. Spiteri, P., Ho, S., & Lee, Y. L. (2007). Assessment Of Bending Fatigue Limit For Crankshaft Sections With Inclusion Of Residual Stresses. International Journal Of Fatigue, 29(2), 318-329. Https://Doi.Org/10.1016/J.Ijfatigue.2006.03.009
[14]. Ko, Y. S., Park, J. W., Bhan, H. O., Park, H., & Lim, J. D. (2005). Fatigue Strength And Residual Stress Analysis Of Deep Rolled Crankshafts (No. 2005-01-0988). Sae Technical Paper. Https://Doi.Org/10.4271/2005-01-0988
[15]. Ho, S., Lee, Y. L., Kang, H. T., & Wang, C. J. (2009). Optimization Of A Crankshaft Rolling Process For Durability. International Journal Of Fatigue, 31(5), 799-808 Https://Doi.Org/10.1016/J.Ijfatigue.2008.11.011
[16]. Williams, J., & Fatemi, A. (2007). Fatigue Performance Of Forged Steel And Ductile Cast Iron Crankshafts. Sae Transactions, 339-349.
[17]. Villalva, S. G., & Junior, E. G. F. (2010, October). Correlation Between Cae And Experimental Fatigue Bench Tests For Automotive Crankshafts. In Sae Brasil 2010 Congress And Exhibit (No. 2010-36-0255). Https://Doi.Org/10.4271/2010-36-0255
[18]. Baragetti, S., Cavalleri, S., & Terranova, A. (2010). A Numerical And Experimental Investigation On The Fatigue Behavior Of A Steel Nitrided Crankshaft For High Power Ic Engines. Journal Of Engineering Materials And Technology, 132(3). Https://Doi.Org/10.1115/1.4001834
[19]. Çevik, G., & Gürbüz, R. (2013). Evaluation Of Fatigue Performance Of A Fillet Rolled Diesel Engine Crankshaft. Engineering Failure Analysis, 27, 250-261. Https://Doi.Org/10.1016/J.Engfailanal.2012.07.026
[20]. Amaral, D. C., Alliprandini, D. H., Forcellini, F. A., De Toledo, J. C., Da Silva, S. L., Scalice, R. K., & Rozenfeld, H. (2017). Gestão De Desenvolvimento De Produtos. Saraiva Educaçao Sa.
[21]. Rao, Singiresu S. (2009) Vibrações Mecânicas.[Sl].